

## Laser Induced Breakdown Spectroscopy for Classification of High Energy Materials using Elemental Intensity Ratios

Sunku Sreedhar\*, Manoj Kumar Gundawar\*, and S. Venugopal Rao

Advanced Centre of Research in High Energy Materials, University of Hyderabad, Hyderabad-500 046, India

\*E-mail: manojsp@uohyd.ernet.in

### ABSTRACT

A simple, yet efficient, methodology is proposed to classify three high energy materials (HEMs) with diverse composition using nanosecond laser induced breakdown spectroscopic data. We have calculated O/N, N/H, and O/H elemental peaks ratios using a ratiometric method. The present work describes a novel way to construct 1D, 2D, and 3D classification model using the above mentioned ratios. Multivariate statistical methods are followed for construction of the classification models. A detailed procedure for classification of three different HEMs is presented here.

**Keywords:** Laser induced breakdown spectroscopy, high energy materials

### 1. INTRODUCTION

Laser induced breakdown spectroscopy (LIBS), an emerging tool for multi-elemental analysis, has specific advantages compared to other techniques like inductive coupling plasma mass spectrometry, atomic absorption spectroscopy and atomic emission spectroscopy<sup>1-3</sup>. LIBS technique employs a pulsed laser (typically nanosecond) to produce breakdown on the surface of sample to be examined. A hot dense plasma is formed post the breakdown. The hot plasma in the process of cooling emits radiation<sup>1-3</sup>. The emitted light is collected with a spectrometer and the collected spectrum consists of several sharp peaks characteristic of elemental and molecular species present in the sample. Exact assignment of these spectral lines is performed with comparison of the available standard atomic emission lines from NIST database<sup>4</sup>. The analysis of LIBS data (line intensities) combined with various statistical methods<sup>5-8</sup> provide plethora of opportunities for identification/discrimination of high energy materials (HEMs). However, the detection mechanism, if carried out in ambient air, is ambiguous because of the contribution from atmospheric constituents such as Hydrogen, Nitrogen, and Oxygen<sup>9</sup>. Recent studies proved that it is possible to reduce these affects to a large extent by using dual pulses<sup>10-12</sup>. There has been considerable progress over the last two decades to discriminate HEMs, chemical, and biological warfare samples using multivariate techniques and several other methodologies<sup>10-23</sup>. LIBS technique equipped with multivariate statistics has found intensive applications in the fields of explosives<sup>13-24</sup>, minerals<sup>25-26</sup>, and in pharmaceuticals<sup>27-28</sup>. Some research groups have successfully performed classification based on elemental intensity ratios obtained in the LIBS spectra<sup>29-31</sup>. Rai<sup>29</sup>, *et al.* have characterized organic compounds 4-nitroaniline and 4-nitrotoluene by measuring

the intensity of atomic lines. Anzano<sup>30</sup>, *et al.* has classified several sets of polymers, successfully, based on C, CN, H, and O ratios. Tran<sup>31</sup>, *et al.* have performed qualitative and quantitative determination of major elements and their ratios in solid organic compounds.

In this paper we present our results from the classification studies of commonly used three inorganic nitrogen rich HEMs, Ammonium Perchlorate ( $NH_4ClO_4$ ) [AP], Boron Potassium Nitrate ( $BKNO_3$ ) [BPN], and Ammonium Nitrate ( $NH_4NO_3$ ) [AN] based on a ratiometric method. AP and AN are generally used as oxidizers in solid rocket propellants. BPN is used as a primary explosive in rocket propellants and improvised explosive devices. We attempt to explain the classification mechanism of above mentioned three molecules, possessing distinct ratios of O/N, H/N and O/H, based on ratiometric method. In general, stoichiometric ablation is assumed in LIBS and other laser ablation techniques. This assumption implies that the ablated volumetric mass represents the exact composition of sample constituents. The ratios can be determined by using the emission lines intensities in the LIBS spectra<sup>19</sup>. Based on the ratios obtained, different classification models, viz. one ratio (1D), two ratios (2D) and three ratios (3D) were developed. Multivariate statistical distribution methods were used in classification along with the calculated ratios. The classification was best achieved with 2D and 3D models. Hydrogen, Nitrogen and Oxygen are the commonly available elements in most of the HEMs. These elemental spectral features appear in the spectral range of 600 nm - 900 nm. We demonstrate that the data collected in this small spectral window could be sufficient for classification of such samples. Using these elemental peaks we have successfully demonstrated the classification models for three HEMs.

Received 1 July 2013, revised 4 April 2014, online published 21 July 2014

Though the methodology explained here is applied for only three samples this approach could be generalized and possibly used for classification of other potentially dangerous HEMs.

## 2. EXPERIMENTAL DETAILS

Figure 1. shows the schematic of LIBS experimental setup. In our studies second harmonic generated pulses from a Nd:YAG laser (Innolas, Spitlite-1300) with 7 ns pulse duration and a repetition rate of 10 Hz were used. The size of the laser beam at exit was 6.5 mm diameter. The laser pulses were focused using an 80 mm focal length lens on the sample. The beam waist was estimated to be  $\sim 20 \mu\text{m}$ , corresponding to peak intensity of  $>100 \text{ GW/cm}^2$ . These intensities were sufficient for the stoichiometric ablation. The depth of focus of laser beam was  $\sim 1.2 \text{ mm}$ . The sample surface was kept at a distance of 1 mm above the focus, such that peak intensities were below the breakdown threshold for air. At this point the spot size was estimated to be  $\sim 80 \mu\text{m}$ . The sample was mounted on an X-Y translation stage with a resolution of  $0.5 \mu\text{m}$ . It was ensured that each laser pulse interacts with the fresh area of the sample. The emission was captured with a gated spectrometer (ANDOR, Mechelle spectrograph ME5000, coupled to an ANDOR iSTAR DH734 ICCD) with a resolving power of 5000. A collection lens system (ANDOR, ME-OPT-8007 UV-NIR light collector) was used to collect the plasma light, the light directly coupled to a  $400 \mu\text{m}$  core diameter fiber which is directly connected to the spectrometer. Circular pellets of  $\sim 20 \text{ mm}$  diameter were prepared by filling the sample in a die and then applying a pressure of eight tones for a period of 10 min.

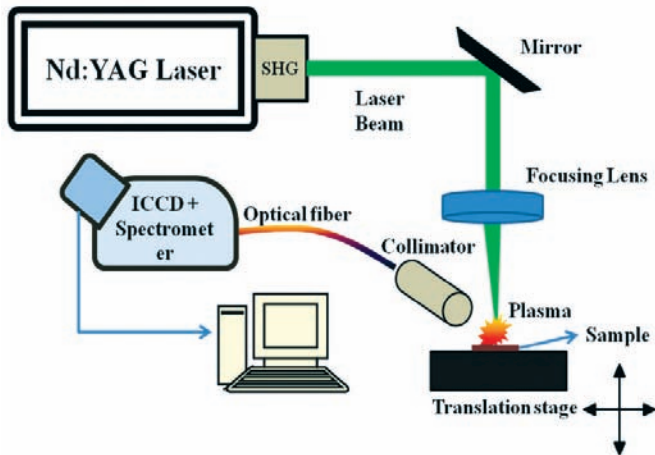


Figure 1. LIBS experimental setup using ns pulses.

## 3. RESULTS AND DISCUSSION

### 3.1 Spectral Analysis

Figures 2(a)-2(c) illustrate the typical LIBS spectra of AP, BPN, and AN accumulated over ten acquisitions, collected with a gate delay of 1000 ns and gate width of 1000 ns. The spectra consisted of several discrete peaks, which have been assigned to corresponding elements using the NIST database. Typical signature peaks of O (777.31 nm, 844.72 nm), H (656.20 nm), N (742.50 nm, 744.34 nm, 746.91 nm, 818.58 nm, 821.69 nm, and 868.18 nm) were observed in all the samples. Cl (837.68 nm) and K (767.6 nm, 769.1 nm) lines were observed in AP and

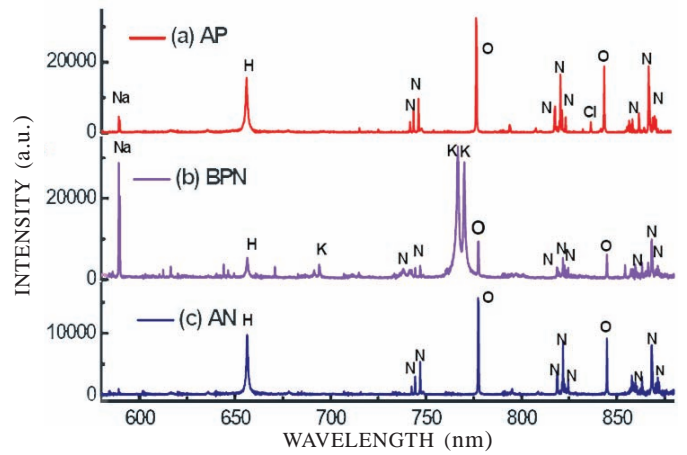


Figure 2. LIBS spectra of AP, BPN and AN samples using nanosecond laser excitation. Data was recorded with 10 accumulations with 1000 ns gate width and 1000 ns gate delay of ICCD spectrometer.

BPN samples, respectively.  $\text{BKNO}_3$  is a mixture with boron and potassium nitrate as its main ingredients and the presence of hydrogen peak in the spectra may either be due to the binder used in composition or an impurity. Spectral signatures of other impurities like *Mg*, *Fe*, *Ca*, and *Na* were also identified.

### 3.2 Measurement of Plasma Parameters

The intensity of each line can be represented by the Eqn. (1)

$$I_{ij}^z = \frac{1}{4\pi} \frac{hc N^z g_i A_{ij}}{\lambda_{ij} U^z(T)} \exp\left(-\frac{E_i^z}{k_B T}\right) \quad (1)$$

In the Eqn. (1),  $\tilde{I}_{ij}^z$  represents line intensity of a particular atomic or ionic line in the spectra,  $U^z(T)$  is the partition function,  $N^z$  is the number density of species  $z$  in the plasma;  $g_i$  and  $A_{ij}$  are statistical weights and transition probability of the upper energy level respectively;  $k$  is Boltzmann constant and  $E_i$  is the energy of upper energy level transition.  $T$  is plasma temperature. Using these intensity lines, we can determine plasma parameters such as temperature and electron density. Using these parameters local thermodynamic equilibrium (LTE) can be validated for the LIBS plasma<sup>1-3</sup>. The plasma temperature can be determined using Saha-Boltzmann method. To obtain a reliable estimate of plasma temperature from Boltzmann plot, it is essential to choose atomic lines, which are clearly separated from other adjacent atomic line<sup>32</sup>. Equation (1) can be rewritten in the form of Eqn. (2).

$$\ln\left(\frac{I_{ij}^z \lambda_{ij}}{g_i A_{ij}}\right) = \left(-\frac{1}{k_B T} E_i^z\right) + \ln\left(\frac{1}{4\pi} \frac{hc N^z}{U^z(T)}\right) \quad (2)$$

To calculate Boltzmann plot, spectral lines belonging to same atomic species or corresponding ionic species of element can be chosen. The plot can be drawn between upper energy level of the spectral transition line and  $\ln\left(\frac{I_{ij}^z \lambda_{ij}}{g_i A_{ij}}\right)$  of the corresponding peak. Obtained points are fitted to a straight line.

The slope of that line is directly proportional to  $\left(\frac{1}{k_B T}\right)$ ; from

which can obtain temperature information<sup>32</sup>. We have used Nitrogen atomic spectral lines for calculating the temperature. The values of temperature calculated for all the samples were in the range of 6000 K to 8000 K. Electron density was obtained from Eqn. (3). Validity of local thermodynamic equilibrium (LTE) condition was performed using Mc-Whirter Criterion as mentioned in Eqn. (3).  $N_e$  is the electron density;  $\Delta\lambda$  is the FWHM of spectral line and  $\omega$  is the impact parameter of that level. The Oxygen peak at 777.31 nm was used for the estimation of the electron density. Typical values obtained were  $\sim 10^{17} \text{ cm}^{-3}$ .

$$N_e \approx \left( \frac{\Delta\lambda}{2\omega} \right) \times 10^{16} \quad (3)$$

$$N_e \geq 1.6 \times 10^{12} T^{1/2} \Delta E^3 \quad (4)$$

The concentration of species can be estimated if the plasma obtained is optically thin plasma and also the condition of Stoichiometric ablation and LTE are satisfied<sup>32,34</sup>. The state of LTE will be best achieved typically after 1  $\mu\text{s}$  of plasma formation for ns laser produced plasmas. At this time the plasma will be in cooling stage<sup>1-3</sup>. Therefore, we had recorded all spectra with three samples with the gate delay of 1  $\mu\text{s}$  and a gate width of 1  $\mu\text{s}$ . Assumption of LTE is valid in the present experiment since the estimated electron densities obtained for our LIBS data satisfied the Mc-Whirter criterion. The intensities which we used were sufficient for stoichiometric ablation. After the fulfilment of all conditions we proceeded with the actual calculations.

### 3.3 Ratiometric Analysis using Elemental Atomic Peaks

Considering the area under the peaks ( $I_{ij}$ ), the density of the species was calculated as  $(I_{ij}/A_{ij}g_i)$ . This quantity  $(I_{ij}/A_{ij}g_i)$  was calculated for each individual lines of O (777.31 nm and 844.7 nm), N (742.5 nm, 744.34 nm, 746.91 nm, and 818.6 nm) and H (656.20 nm). The ratios O/N, N/H and O/H were obtained by dividing the  $(I_{ij}/A_{ij}g_i)$  of each line. All possible ratios were calculated using these peaks. For each sample these ratios were obtained from an average of several independent measurements. The appraised ratios for all three samples are listed in Table 1. Out of all the ratios, the O/N ratios calculated with O (777.31 nm) and N (744.34 nm, 746.91 nm) lines were found to be closer to the stoichiometric ratio. The values of two above mentioned ratios for AP were  $3.78 \pm 0.42$ ,  $3.99 \pm 0.32$ , for  $\text{BKNO}_3$  were  $3.09 \pm 0.78$ ,  $3.14 \pm 0.40$ , and for AN were  $2.91 \pm 0.16$ ,  $2.8 \pm 0.13$ . The other ratios obtained for H/N and O/H were also calculated with the combination of spectral lines shown in Table 1. These ratios could make possible classification at a primary level. Since all the measurements were performed in ambient air the ratios could be improved with inert gas purging on the sample surface. But in real applications we cannot afford to use purge gas. Based on the obtained ratiometric results we implemented simple statistical methods using these ratios to improve the ability of classifying three samples significantly.

### 3.4 Method of Classification

The model has been constructed with the obtained ratios of O(777.31 nm)/N(746.91 nm), H(656.20 nm)/N(746.91 nm), and O(777.31 nm)/H(656.20 nm) ratios. For all the three

Table 1. Calculated intensity ratios for three samples

Ratio	Stoi.	AP	Stoi.	BPN	Stoi.	AN
O777.31/N742.50	4	3.96±0.62 (15.55)	3	2.24±0.48 (21.47)	1.5	3.04±0.49 (16.14)
O777.31/N744.34	4	3.78±0.42 (10.98)	3	3.09±0.78 (25.17)	1.5	2.90±0.16 (5.43)
O777.31/N746.91	4	3.99±0.32 (8.03)	3	3.14±0.40 (12.86)	1.5	2.84±0.13 (4.44)
O777.31/N818.58	4	3.85±0.63(16.34)	3	2.79±0.14 (5.18)	1.5	2.84±0.31 (10.98)
O844.72/N742.50	4	2.80±0.32 (11.52)	3	1.36±0.77 (56.60)	1.5	2.49±0.43 (17.21)
O844.72/N744.34	4	2.67±0.09 (3.39)	3	2.62±0.65 (24.93)	1.5	2.37±0.17 (6.99)
O844.72/N746.91	4	2.83±0.18 (6.52)	3	2.67±0.28 (10.69)	1.5	2.32±0.12 (4.98)
O844.72/N818.58	4	2.71±0.26 (9.47)	3	2.39±0.24 (10.26)	1.5	2.32±0.26 (11.15)
H656.20/N742.50	4	2.38±0.36 (15.03)	-	0.95±0.57 (59.76)	2	2.38±0.44 (18.36)
H656.20/N744.34	4	2.26±0.14 (6.37)	-	1.79±0.42 (23.60)	2	2.27±0.21 (9.31)
H656.20/N746.91	4	2.39±0.20 (8.40)	-	1.82±0.21 (11.64)	2	2.23±0.20 (8.92)
H656.20/N818.58	4	2.30±0.25 (11.08)	-	1.63±0.10 (6.40)	2	2.23±0.30 (13.49)
O777.31/H656.20	1	1.68±0.22 (12.85)	-	1.72±0.05 (2.62)	.75	1.28±0.09 (7.05)
O844.72/H656.20	1	1.18±0.06 (5.14)	-	1.46±0.09 (6.37)	.75	1.05±0.05 (4.92)

Values are in format – Mean ± SD (%RSD)

Stio: Actual stoichiometry ratio of the sample, Mean: average value of several independent measurements, SD: standard Deviation, %RSD: Relative standard deviation Percentage

samples each ratio versus the number of independent trials is plotted in Fig. 3. In Figs. 3(a)-3(c) scattered points for each trial obtained from different samples occupy a specific region of Y-axis. It is evident that more than 60% points from same sample are grouped in a region along Y-axis. The classification of three samples using one ratio (1D) is explained with the help of box plots. We had applied probability density function for experimental points to draw the box plots. Such plots for each ratio are plotted and are depicted on the right hand side of each graph. It is apparent from Figs. 3(a)-3(c) that distribution of each ratio has its own characteristic mean position, interquartile ranges and a box width. In one dimensional ratio approach the scatter plot and box plot present visualization of the distribution. The criterion for exact classification of the samples will not be fulfilled because of the presence of few intersecting points. To overcome this situation we had taken two ratios for discrimination of samples to construct a 2D model.

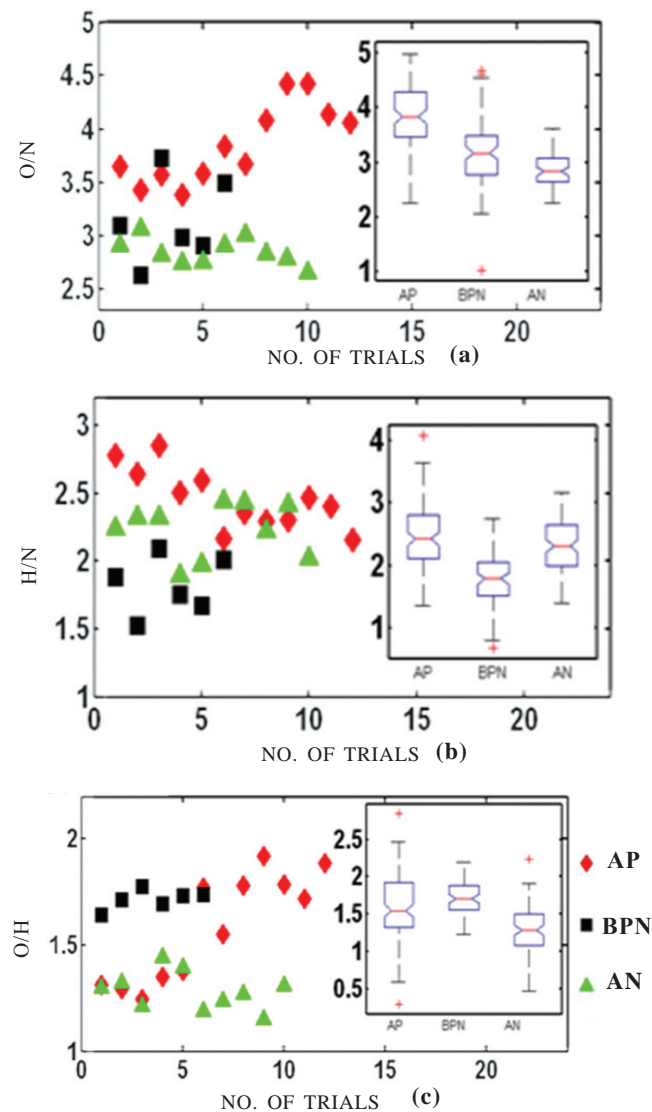


Figure 3. Scattered plots drawn with number of trials vs experimentally obtained ratio value for each elemental ratio for (a) O/N ratio, (b) H/N ratio, and (c) O/H ratio. The box plot depicted right side corner of each scatter plot is deduced from probability distribution function for each ratio.

Figure 4 illustrates the classification based on a two dimensional ratio approach. With the combination of two ratios out of possible three a total of three graphs are plotted (4(a) O/N and H/N, 4(b) O/N and O/H and 4(c) H/N and O/H). It is apparent that the points corresponding to each sample are scattered in a group. To apply the multivariate normal distribution for these grouped regions 1000 points were randomly generated in accordance with the experimental points<sup>35,36</sup>. Since the variables (ratios) are two, bivariate normal distribution method was applied for our data to generate the required random points. The bivariate normal distribution is derived from the statistical variables which are the means of two variable  $\mu_1$  and  $\mu_2$  and covariance  $\sigma[2 \times 2]$  matrix elements. The multivariate normal distribution is done based on the Eqn. (5).

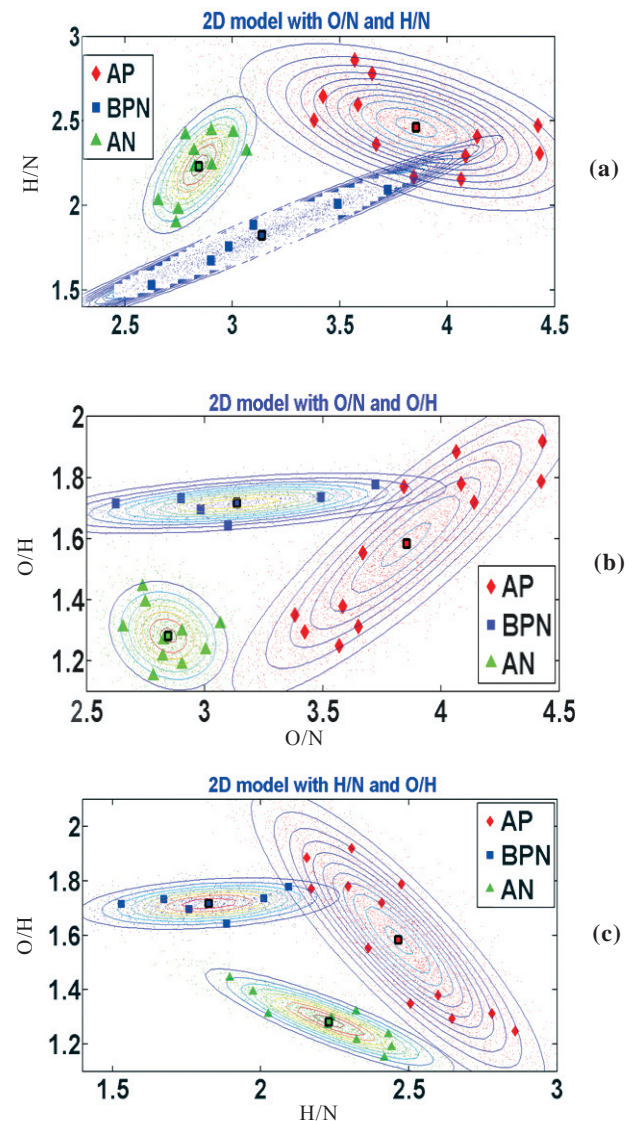
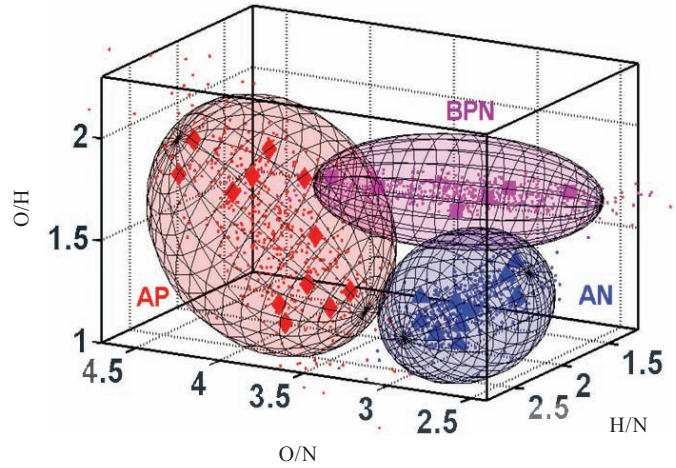


Figure 4. Classification of 3 samples using two ratios (2D) combinations. (a) is drawn with O/N and H/N ratios, (b) O/N and H/N ratios, and (c) H/N and O/H ratios. The experimental points (bigger size) corresponds to each sample are represented with different symbols and colors. Scattered small points in the regions are randomly generated points for a particular sample.

$$f(X : \mu, \sigma) = \left( \frac{1}{(2\pi)^{n/2} |\Sigma|^{1/2}} \right) \exp \left[ -(X - \mu)' \Sigma^{-1} (X - \mu) \right] \quad (5)$$

The central point of distributed region was at the intersection of two means (black color outer line point at middle of the each 2D region). The spread of distribution along two axes is determined by on-diagonal elements of the covariance matrix. If the diagonal elements of covariance matrix are equal, distribution will be in the form of circle else it takes the form of an ellipse. For a particular distribution region, along both the X and Y directions, the spread of elliptical contours were  $2\sqrt{\sigma_{ii}}$ . The upper off-diagonal element decides the orientation of elliptical lines in distribution<sup>37</sup>. The elliptical contour lines were drawn by connecting equal probability points in the direction of covariance elements. Three distribution regions were obtained corresponding to three samples which are shown in the plots of Fig. 4. The obtained experimental points are on the boundaries of elliptical contours. These distribution regions along with the contours endow classification of these samples. In Fig. 4(a) the classification was obtained with O/N and H/N ratios and we observed that there was a slight interference between BPN and AP distributions and a small intersection for AP and AN regions. As shown in Fig. 4(c) the interference between AP and BPN samples region decreased with 2D model for the ratios O/H and H/N and there was no intersection with the AP and AN regions. The classification was further improved with O/N and O/H ratios. In Fig. 4(b) we noticed lesser interference between AP and BPN regions as compared to other two 2D models and also the separation between AP and AN regions was improved. From this we concluded that the two ratio 2D model of classification provides a superior discrimination compared to the single ratio method. Amongst all two dimensional classifications shown in the Fig. 4(b) the plot between ratios O/N and O/H gave better discrimination of samples.

Further we constructed a three dimensional model using all the three elemental ratios. Figure 5 shows the three dimensional plot using the three ratios O/N, O/H and H/N. The scattered points corresponding to each sample confined to a specific volume region in three dimensional space. The same multivariate normal distribution technique based on Eqn. (5) was applied. The points were generated with multivariate method with the mean and covariance  $\sigma [3 \times 3]$  matrix of three variables (three ratios). The points surrounded with actual experimental ratio points are shown in Fig. 5. In this case the locus of equal probability points represents an ellipsoid. The spread of ellipsoid in three directions will be decided by three on-diagonal elements of covariance matrix and spread will be  $2\sqrt{\sigma_{ii}}$ . Three ellipsoids were drawn using these methods for each sample. We observe that for a particular ellipsoid containing the experimentally obtained points (denoted with thick colored square symbols) and statistically generated random points (denoted with small scattered colored symbols) were confined within the ellipsoid. These ellipsoids are significantly free from intersection from other ellipsoids corresponding to a different sample. These ellipsoids provide better discrimination for all the three samples.



**Figure 5.** Classification of three samples using three ratios method (3D model). Each ellipsoid region represents a sample distribution space named beside it. The experimental points (bigger size) obtained from the samples are shown in different symbols and colors. Small scattered points with a particular color were randomly generated using multivariate distribution.

Table 2 shows the calculated distances between means of different sample regions. The Euclidian distance was obtained with inner product of two mean vectors for any two regions. Larger distance represents the sample regions separated largely with one another and therefore classification of the samples would be superior. We obtained large separation distances for the regions with O/N and H/N ratios (Fig. 4(a)) but regions are poorly intersecting. With O/N and O/H ratios model (Fig. 4(b)) the separation distance obtained was also large with very slight interference among the region boundaries. The distance between the medians for all the three samples volumes in 3D model was also calculated. As compared to 2D model, the separation distance between sample medians was higher in 3D model meaning regions are separated significantly. Comparing the 2D and 3D models presented we can conclude that 3D model provided reliable classification where as 2D model was easy to apply. Clubbing these multi-dimensional models along with multivariate distribution methods has significantly improved the accuracy of classification.

**Table 2.** Euclidian distances calculated between the mean points of the regions in all the models

	AP to BPN	AP to AN	BPN to AN
<b>2D Model</b>			
O/N and H/N	0.96	1.04	0.50
O/N and O/H	0.73	1.05	0.52
H/N and O/H	0.65	0.38	0.59
<b>3D Model</b>			
O/N, H/N and O/H	0.97	1.08	0.66

#### 4. CONCLUSIONS

Three HEMs were discriminated using the ratiometric approach. A marginal discrimination was obtained with 1D classification model using individual O/N, H/N, and O/H ratios. Good quality discrimination was obtained with 2D classification using two different ratios. Best classification

was achieved using three ratios taken together and plotted (3D model) without any intersecting points. The successful implementation of multivariate discrimination techniques to the models has increased the level of accuracy of classification. Unambiguous distinction was achieved with the simple elemental ratios using these schemes. The described method could be implemented for classification other explosives possessing similar elemental composition. Further studies are in progress towards achieving this goal.

#### ACKNOWLEDGEMENTS

Authors acknowledge the financial support from Defence Research & Development Organisation, India.

#### REFERENCES

- Miziolek, A.W.; Palleschi, V. & Schechter, I. Laser-induced breakdown spectroscopy (LIBS): Fundamentals and Applications. Cambridge University Press, 2006.
- Cremers, D.A. & Radziemski, L.J. Handbook of laser-induced breakdown spectroscopy. Wiley, 2006.
- Singh, J.P. & Thakur, S.N. Laser-induced breakdown spectroscopy. Elsevier, Amsterdam, 2007.
- NIST database of atomic spectral data. <http://physics.nist.gov/PhysRefData/ASD>.
- Harmon, R.S.; De Lucia, F.C.; Winkel Jr, R.J.; LaPointe, A.; Grossman, S.; McNesby, K.L. & Miziolek. LIBS: A new versatile, field deployable, real-time detector system with potential for landmine detection. *SPIE.*, 2003, **5089**(2), 1065-1077.
- Lopez-Moreno, C.; Palanco, S.; Laserna, J.J.; DeLucia Jr, F. & Whitehouse, A. Test of a stand-off laser-induced breakdown spectroscopy sensor for the detection of explosive residues on solid surfaces. *J. Anal. At. Spectrom.*, 2006, **21**(1), 55-60.
- Gottfried, J.L.; De Lucia Jr, F.C.; Munson, C.A. & Miziolek, A.W. Standoff detection of chemical and biological threats using laser-induced breakdown spectroscopy. *Appl. Spectrosc.*, 2008, **62**(4), 353-363.
- Gonzalez, R.; Lucena, P.; Tobarria, L.M. & Laserna, J.J. Standoff LIBS detection of explosive residues behind a barrier. *J. Anal. At. Spectrom.*, 2009, **24**(8), 1123-1126.
- Brown, C.G.; Baudelet, M.; Bridge, C.; Fisher, M.K.; Sigman, M.; Dagdigian, P.J. & Richardson, M. Atmosphere issues in detection of explosives and organic residues. *SPIE.*, 2009, **7304**, 73041D.
- Babushok, V.I.; Delucia Jr, F.C.; Gottfried, J.L.; Munson, C.A. & Miziolek, A.W. Double pulse laser ablation and plasma: Laser induced breakdown spectroscopy signal enhancement. *Spectrochim. Acta. Pt. B*, 2006, **61**(9), 999-1014.
- De Lucia Jr., F.C.; Gottfried, J.L.; Munson, C.A. & Miziolek, A.W. Double pulse laser-induced breakdown spectroscopy of explosives: Initial study towards improved discrimination. *Spectrochim. Acta Pt. B*, 2007, **62**(12), 1399-1404.
- Gottfried, J.L.; De Lucia Jr., F.C.; Munson, C.A. & Miziolek A.W. Double-pulse standoff laser-induced breakdown spectroscopy for versatile hazardous materials detection. *Spectrochim. Acta Pt. B*, 2007, **62**(12), 1405-1411.
- Gottfried, J.L.; De Lucia, Jr, F.C.; Munson, C.A. & Miziolek, A.W. Strategies for residue explosives detection using laser-induced breakdown spectroscopy. *J. Anal. At. Spectrom.*, 2008, **23**(2), 205-216.
- Sreedhar, S.; Manoj Kumar, G.; Ashwin Kumar, M.; Prem Kiran, P.; Tewari, S. P. & Venugopal Rao, S. Femtosecond and nanosecond laser induced breakdown spectroscopic studies of NTO, HMX, and RDX. *Spectrochim. Acta Pt. B*, 2013, **79-80**, 31-38.
- Sreedhar, S.; Nageswara Rao E.; Manoj Kumar, G.; Tewari, S.P. & Venugopal Rao, S. Molecular formation dynamics of 5-nitro-2,4-dihydro-3H-1,2,4-triazol-3-one, 1,3,5-trinitroperhydro-1,3,5-triazine, and 2,4,6-trinitrotoluene in air, nitrogen, and argon atmospheres studied using femtosecond laser induced breakdown spectroscopy. *Spectrochim. Acta Pt. B*, 2013, **87**, 121-129.
- Sreedhar, S.; Nageswara Rao E.; Manoj Kumar, G.; Tewari, S. P. & Venugopal Rao, S., Discrimination methodologies using femtosecond LIBS and correlation techniques. *SPIE*, 2013, **8726**, 87260H-1
- Sreedhar, S.; Nageswara Rao E.; Manoj Kumar, G.; Tewari, S. P. & Venugopal Rao, S., Investigation of molecular and elemental species dynamics in NTO, TNT, and ANTA using femtosecond LIBS technique. *SPIE*, 2013, **8710**, 871012-1.
- Venugopal Rao, S.; Sreedhar, S.; Kumar, M.A.; Kiran, P.P.; Tewari, S.P & Kumar, G.M.; Laser Induced Breakdown Spectroscopy of high energy materials using nanosecond, picosecond, and femtosecond pulses: Challenges and opportunities. *SPIE*, 2011, **8173**, 81731A.
- Sreedhar, S.; Ashwin Kumar M.; Manoj Kumar G.; Prem Kiran P.; Tewari, S. P. & Venugopal Rao S, Stoichiometric analysis of inorganic compounds using laser-induced breakdown spectroscopy with gated and non-gated spectrometers. *ISRN Optics*, 2012, Article ID 631504, 8 pages. DOI: 10.5402/2012/631504
- Lazic, V.; Palucci, A.; Jovicevic, S. & Carpanese, M. Detection of explosives in traces by laser induced breakdown spectroscopy: Differences from organic interferences and conditions for a correct classification. *Spectrochim. Acta Pt. B*, 2011, **66**(8), 644-655.
- Gottfried, J.L.; De Lucia Jr., F.C.; Munson, C.A. & Miziolek, A.W. Laser-induced breakdown spectroscopy for detection of explosives residues: A review of recent advances, challenges, and future prospects. *Anal. Bioanal. Chem.*, 2009, **395**(2), 283-300.
- Gottfried, J.L. Discrimination of biological and chemical threat stimulants in residue mixtures on multiple substrates. *Anal. Bioanal. Chem.*, 2011, **400**(10), 3289-3301.
- Baudelet, M.; Yu, J.; Bossu, M.; Jovelet, J.; Wolf, J.-P.; Amodeo, T.; Frejafon, E. & Laloi, P.; Discrimination of microbiological samples using femtosecond laser-induced breakdown spectroscopy. *Appl. Phys. Lett.*, 2006, **89**, 163903-905.
- Lazic, V.; Palucci, A.; Jovicevic, S.; Poggi, C. & Buono,

- E. Analysis of explosive and other organic residues by laser induced breakdown spectroscopy. *Spectrochimica Acta Pt. B*, 2009, **64**(10), 1028-1039.
25. Clegg, S.M.; Sklute, E.; Dyar, M.D.; Barefield, J.E. & Wiens, R.C. Multivariate analysis of remote laser-induced breakdown spectroscopy spectra using partial least squares, principal component analysis, and related techniques. *Spectrochim. Acta Pt. B*, 2009, **64**(1), 79-88.
  26. Laville, S.; Sabsabi, M. & Doucet, F.R. Multi-elemental analysis of solidified mineral melt samples by laser-induced breakdown spectroscopy coupled with a linear multivariate calibration. *Spectrochim. Acta Pt. B*, 2007, **62**(12), 1557-566.
  27. Myakalwar, A.K.; Sreedhar, S.; Barman, I.; Dingari, N.C.; Rao, S.V.; Kiran, P.P.; Tewari, S.P. & Kumar, G.M. Laser-induced breakdown spectroscopy-based investigation and classification of pharmaceutical tablets using multivariate chemometric analysis. *Talanta*, 2011, **87**, 53-59.
  28. Dingari, N.C.; Barman, I.; Kumar, M.A.; Tewari, S.P. & Kumar, G.M. Incorporation of support vector machines in the LIBS toolbox for sensitive and robust classification amidst unexpected sample and system variability. *Analytical Chemistry*, 2012, **84**(6), 2686-2694.
  29. Rai, S.K.; Rai, A.K. & Thakur, S.N. Identification of nitro-compounds with LIBS. *Appl. Phys. B*, 2008, **91**(3-4), 645-650.
  30. Anzano, J.; Lasheras, R.-J.; Bonilla, B. & Casas, J. Classification of polymers by determining of  $C_1:C_2$ :CN: H:N:O ratios by laser-induced plasma spectroscopy (LIPS). *Polymer Testing*, 2008, **27**(6), 705-710.
  31. Tran, M.; Sun, Q.; Smith, B.W. & Winefordner, J.D. Determination of C:H:O:N ratios in solid organic compounds by laser-induced plasma spectroscopy. *J. Anal. At. Spectrom.*, 2001, **16**(6), 628-632.
  32. Griem, H.R. Principles of plasma spectroscopy. Cambridge University Press, Cambridge, 1997.
  33. Cristoforetti, G.; De Giacomo, A.; Dell'Aglio, M.; Legnaioli, S.; Tognoni, E.; Palleschi, V. & Omenetto, N. Local thermodynamic equilibrium in laser-induced breakdown spectroscopy: Beyond the McWhirter criterion. *Spectrochim. Acta Pt. B*, 2010, **65**(1), 86-95.
  34. Capitelli, M.; Capitelli, F. & Eletsii, A. Non-equilibrium and equilibrium problems in laser-induced plasmas. *Spectrochim. Acta Pt. B*, 2000, **55** (6), 559-574.
  35. James, M. Classification algorithms. John Wiley & Sons, Inc., 1985.
  36. Marques de Sá, J.P. Applied statistics using SPSS, STATISTICA, MATLAB and R, Springer-Verlag, Hidenberg, 2007.
  37. Lattin, J.; Carroll, J.D. & Green, P.E. Analyzing multivariate data. Cengage Learning India Private Limited. India, 2010.

## CONTRIBUTORS



**Mr S. Sreedhar** received his MSc (Physics) from Vellore Institute of Technology, Vellore, in 2006. Presently pursuing his PhD (Physics) at Advanced Centre of Research on High Energy Materials (ACRHEM), University of Hyderabad, Hyderabad. His research interest includes: Femtosecond and nanosecond laser induced breakdown spectroscopy, nanoparticle generation using laser ablation in liquids, diagnostics of laser induced plasma.



**Dr Manoj Kumar Gundawar** obtained his PhD from University of Hyderabad in 2005. Presently working as Assistant Professor at ACRHEM, University of Hyderabad since 2007. His primary research interest is Laser induced breakdown spectroscopy. He worked as project engineer at Electro Optical Instruments Research Academy, Hyderabad where he was involved in the development of Er doped fiber laser and waveguide fabrication on  $LiNbO_3$ .



**Dr S. Venugopal Rao** obtained his MSc and PhD from University of Hyderabad, India. Presently associated with ACRHEM, University of Hyderabad working towards understanding the interaction of nanosecond, picosecond, and femtosecond laser pulses with high energy materials using various time-resolved spectroscopic techniques such as, ultrafast pump-probe, ultrafast ablation, femtosecond laser induced breakdown spectroscopy and ultrafast laser direct writing. He has more than 150 papers in international journals and refereed conference proceedings. He is recipient of the NASI-SCOPUS young scientist award for the year 2012 in physics.